Passive Damping In EDS Maglev Systems

Maglev2002 Conference PP01104.DOC.
By Donald M. Rote
Argonne National Laboratory

1. Introduction

There continues to be strong interest in the subjects of damping and drag forces associated with electrodynamic suspension (EDS) systems. While electromagnetic drag forces resist the forward motion of a vehicle and therefore consume energy, damping forces control, at least in part, the response of the vehicle to disturbances. Ideally, one would like to reduce the drag forces as much as possible while retaining adequate damping forces to insure dynamic stability and satisfactory ride quality. These two goals turn out to be difficult to achieve in practice. It is well known that maglev systems tend to be intrinsically under damped. Consequently it is often necessary in a practical system design to enhance the damping passively or actively. For reasons of cost and simplicity, it is desireable to rely as much as possible on passive damping mechanisms. In this paper, rough estimates are made of the passive damping and drag forces caused by various mechanisms in EDS systems. No attention will be given to active control systems or secondary suspension systems which are obvious ways to augment passive damping mechanisms if the latter prove to be inadequate.

2. Origins of Passive Damping and Drag Forces

In general, both electromagnetic drag forces and damping forces dissipate energy. Drag forces oppose the propulsion force and are present regardless of whether or not there are disturbances in the vehicle's motion. They can arise from several sources including I^2R losses due to the electromotive forces induced in the guideway lift and guidance coils, eddy currents induced in thick conductors of those coils and in metallic fasteners and guideway structural members including re-enforcing rods (rebar). They can also result from the transfer of energy from electromagnetic coupling between on-board linear generator coils and guideway coils. Since all of these sources of drag force are dependent on the magnetic flux in the air gaps, fluctuations in those air gaps caused by perturbations (vehicle or guideway displacements) will affect the magnitudes of the drag force terms to some extent. Even though the effects of these fluctuations may be relatively small compared to the steady-state drag forces, they are also sources of damping of vehicle oscillations.

In contrast to the steady-state drag forces , damping forces only arise in response to disturbances. The various damping mechanisms can be roughly classified according to whether the primary energy dissipation mechanism is electromagnetic, mechanical, or aerodynamic in nature. Generally, in a practical system, all three of these types of damping mechanisms operate jointly. The mechanisms may be further classified according to whether they are active (i.e. involving the use of control systems incorporating feedback) or passive, and if passive, whether they are naturally occurring (e.g., intrinsic magnetic damping), or enhanced in some way. In the present paper, attention will be focused exclusively on passive electromagnetic damping mechanisms. The principle passive damping mechanisms of interest all involve eddy currents induced in metallic conductors by oscillations of the vehicle in the vertical and lateral directions. These include eddy currents induced in rebar and

guideway-mounted coil conductors by oscillations of the SCM's, and eddy currents induced in vehicle-borne damping plates and coils and cryostat walls by their motions relative to the null-flux lift coils and excited propulsion coils. Due to the complexity of exact solutions to the problems, only approximate methods will be used to evaluate the relative magnitudes of the forces resulting from these various damping mechanisms.

3. Drag Forces and Damping Associated With Eddy Currents Induced in Guideway Conductors

Under steady-state conditions the movement of a vehicle along the guideway exposes the metallic guideway components to time-varying magnetic fields. This exposure induces currents to flow in the lift, guidance and propulsion coils that, in turn, result in the forces that govern the vehicle's position and motion. In addition to producing those forces, the induced currents also result in I^2R losses that heat the coils and cause electromagnetic drag forces. Also during steady-state motion, eddy currents are induced within the crosssections of the rebar and the coil conductors. These eddy currents do not make useful contributions to the propulsion, lift, and guidance forces, but they do add to the drag forces.

3.1 Steady-State Power Dissipation and Associated Drag Forces

Zahn and his students at MIT[1] derived expressions for power dissipated in both magnetic and non-magnetic straight, round conductors exposed to alternating magnetic fields . As noted in Ref. 1, ordinary steel rebar is magnetic and not suitable for use near the magnets used in EDS maglev systems. Hence, only non-magnetic steel rebar will be considered here. According to Ref. 1, in the large skin depth limit (f < 2000 Hz for non-magnetic materials), the dissipated power is given as follows:

In the axial case, i.e., the conductor is oriented parallel to **B**,

$$\langle P \rangle_{axial}(W/m) = 0.25\pi r^4 B_0^2 \sigma \left(\pi f \frac{\mu}{\mu_0} \right)^2 . \qquad (1)$$

and in the transverse case, i.e., when the conductor is oriented perpendicular to **B**,

$$\langle P \rangle_{trans}(W/m) = 0.5\pi r^4 B_0^2 \sigma \left(\pi f \frac{\mu}{\mu_0} \right)^2 \left(\frac{2\mu_0}{\mu + \mu_0} \right)^2 . \qquad (2)$$

where f and B_0 are the frequency and amplitude of the sinusoidal-varying magnetic field caused by a series of vehicle-borne, alternating polarity magnets sweeping past the guideway conductors.

When $\mu \approx \mu_0$, Eqn. (2) is seen to be twice as large as Eqn. (1) for the same values of r, B_0, σ, and f.

Table 1 Properties of Guideway Materials

Material	Permeability (4π e-7)	Conductivity (S/m)	Typical Radius (m)	$\approx B_0$ (T)	Product ($\sigma B^2 r^4$)
Aluminum	1	3.53 e 7	0.00423 to 0.00733	0.83	0.0078 to 0.070
13% Mn Steel	1.01	1.41 e 6	0.00635 to 0.0127	0.06 to 0.6	8.3 e-6 to 0.013

To obtain a rough estimate of the contributions of aluminum conductors and rebar, it is necessary to take into account the orientation and number of conductors used in a practical guideway design For illustrative purposes, the following assumptions are made:

There are four superconducting coils per SCM as shown in Fig. 1b. All are in the same x-z plane at y = 0. (See Fig. 1a for the coordinate system used in this report).
There are three aluminum lift coils per superconducting coil in the guideway (See Fig. 1c). These coils are all in the x-z plane at y = - 0.185 m.

The guideway is assumed to be u-shaped with non-magnetic ($\mu \approx \mu_0$) rebar aligned in the x- and z-directions in the sidewalls and in the x- and y- directions in the guideway base or floor.
Intersecting rebar make no electrical contact. Note, if intersecting rebar made electrical contact, then induced currents would also circulate in the resulting closed circuit loops , which would lead to additional losses.
The rebar in the sidewall are all located in the x-z plane at y = 0.4 m.
The rebar in the floor are all in the x-y plane at z = - 0.475 m.
The variations in the magnetic field seen by the rebar and coil conductors are sinusoidal.

Generally, as a series of magnets sweep past a straight segment of conductor, the segment will see a combination of periodic transverse and axial magnetic field components. Provided that these periodic field components are sinusoidal, Eqns (1) and (2) apply, and can be combined to give

$$\langle P \rangle = 0.5\pi^3 \sigma f^2 r^4 \left[B_T^2 + 0.5 B_A^2 \right], \tag{3}$$

where B_T and B_A are the amplitudes of the transverse and axial fields, respectively. In terms of the Cartesian components of the magnetic field, B_T and B_A are:

$$B_T^2 = B_x^2 + B_y^2 \text{ and } B_A^2 = B_z^2 \quad \text{for the vertical conductor segments in the sidewalls,} \tag{4}$$

$$B_T^2 = B_y^2 + B_z^2 \text{ and } B_A^2 = B_x^2 \quad \text{for the longitudinal segments in the sidewalls and floor, and}$$

$$B_T^2 = B_x^2 + B_z^2 \text{ and } B_A^2 = B_y^2 \quad \text{for the lateral segments in the floor.}$$

The B_X, B_Y, and B_Z components of the field in Eqn. 4 are assumed to be due only to each sequence of four coils constituting each SCM. (That is, of course not strictly valid because the total field seen by the conductors is the sum of all field sources). The fields for each SCM were calculated using a

numerical procedure based on the law of Biot and Savart. The dependence of these field components on position (x) departs from sinusoidal in two respects. Obviously, since there are only four superconducting coils in sequence, the variations with x are aperiodic. Second, because of the rectangular coil geometry, even an infinite sequence of such coils would not produce purely sinusoidal waveforms. Nevertheless, it will be assumed here that the waveforms can be approximated as sinusoidal and that average amplitudes obtained from graphs of each field component vs. position are sufficiently accurate representations for the present estimates.

Essentially, what is being assumed here is that each set of four coils constituting a single SCM interacts with the very long sequence of pieces of guideway rebar (or coil conductor segments) as though there were an infinite sequence of SCM's as well. Physically, this is not an unreasonable assumption because the presence of additional SCM's would not have a large effect on the power dissipation and drag force calculations. However, additional SCM's would directly affect the energy transferred to the guideway metallic components and their resultant temperature rise.

The parameter values used in the calculations are listed in Table 2 for three different cases. The results are summarized in Table 3. The drag force is given by the power dissipation divided by the vehicle velocity. In terms of the power dissipated and the associated drag force, the null-flux coils are the most important followed by the propulsion coils and the rebar. For the combined best cases, the total dissipated power is 93 kW, whereas for the combined worst cases it is 2.01 MW. For a train consisting of 14 cars (30 SCM's), the total loss ranges from 2.8 to 61 MW. Obviously, considerable care is required to minimize these sources of steady-state power loss and drag force.

Table 2 Parameters of a Hypothetical EDS Maglev System With a Null-Flux Coil Suspension System.

	Case 1	Case 2	Case 3
No. of SCM's per bogie	2	2	2
SCM pitch (m)	1.35	1.35	1.35
Null-flux coil pitch (m)	0.45	0.45	0.45
Null-flux coil length (m)	0.35	0.35	0.35
Null-flux coil loop height (m)	0.34	0.34	0.34
No, of turns per coil	**48**	**16**	**48**
No. of insulated strands/conductor	-	-	**7**
Null-flux coil conductor radius (mm)	**4.23**	**7.33**	**1.56**
No. of null-flux coils per SCM	12	12	12
Distance from SCM to Null-flux coil plane	0.185	0.185	0.185
Propulsion coil length	0.3364	0.3364	0.3364
Propulsion coil height	0.6	0.6	0.6
No. of coils per SCM	12	12	12
No. of turns per coil	16	16	16
No. of insulated strands/conductor	-	-	**7**
Propulsion coil conductor radius (mm)	**4.308**	**5.45**	**1.56**
Distance from SCM to propulsion coil plane	0.24	0.24	0.24
Rebar material	13%Mn steel	13%Mn steel	
Rebar radius (m)	**0.00794**	**0.01588**	
Rebar spacing	0.1524	0.1524	
Length of vertical rebar (m)	1.4	1.4	
Exposed length of cross floor rebar (m)	1.75	1.75	
No. of vert. rebar in sidewall/SCM	**108**	**27**	
No. of long. rebar in sidewall/SCM	**30**	**8**	
No. of cross rebar in floor/SCM	**108**	**27**	
No. of long. rebar in floor/SCM	**35**	**8**	

Table 3 Eddy Current Losses in Guideway Components Per SCM at 550 (km/h) (152.8 m/s)

	13%Mn Steel Rebar		Null-Flux Lift Coils		Propulsion Coils	
	Power Lost (kW)	Drag Force (kN)	Power Lost (kW)	Drag Force (kN)	Power Lost (kW)	Drag Force (kN)
Case 1	6.8	0.044	589	3.85	83	0.54
Case 2	27.2	0.178	1770	11.6	213	1.39
Case 3			76	0.50	10	0.065

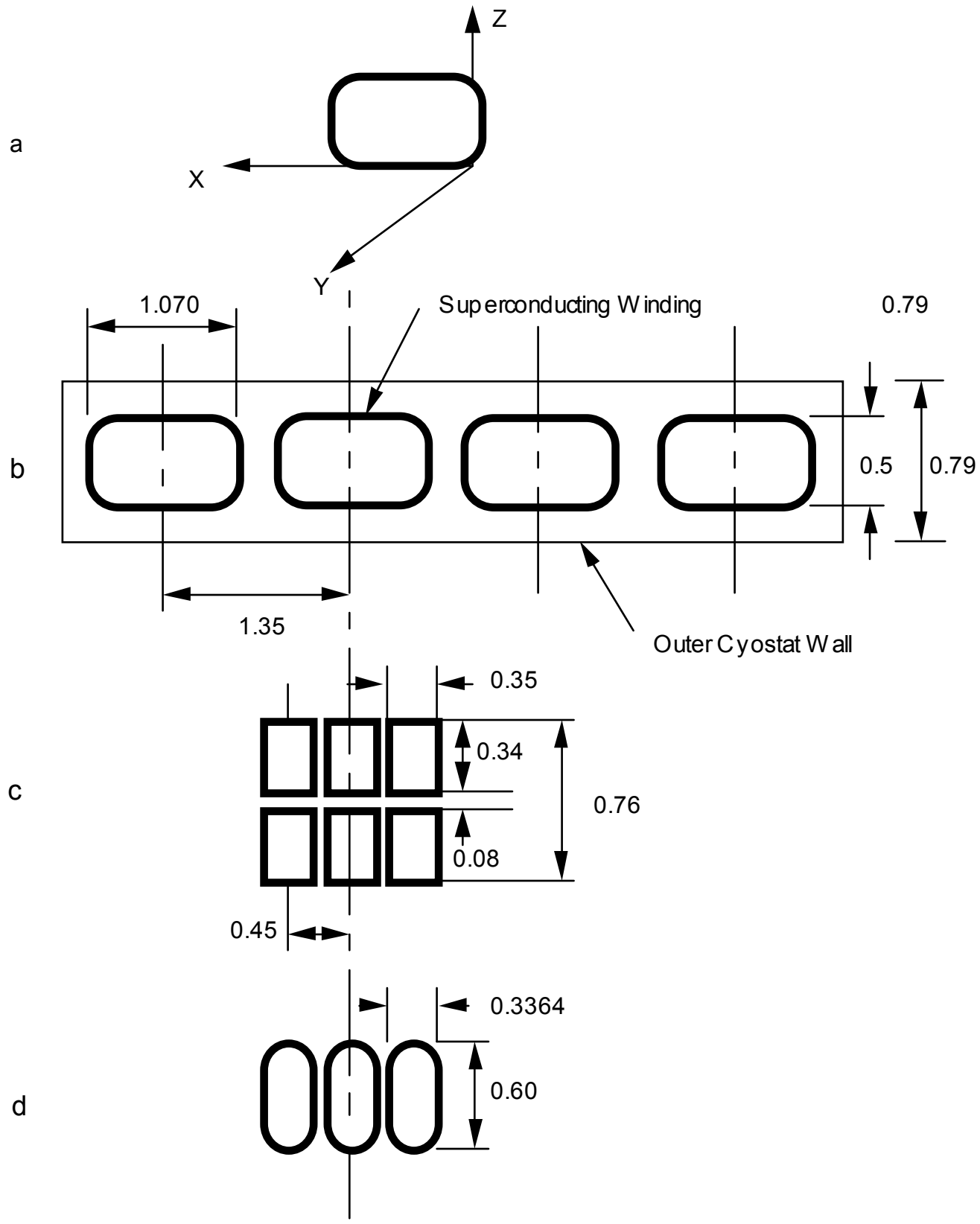

Figure 1. a) Coordinate System; b) Superconducting Magnet with 4 Coils; c) Three Null-Flux Coils Facing Each SCM Coil; d) Three Propulsion Coils Facing Each SCM coil.

3.2 Damping Forces

In the previous section, power dissipation and drag forces due to eddy currents induced in rebar and coil conductors by steady-state motion of the vehicle in the x-direction were estimated. Here, estimates are made of the damping forces associated with the eddy current losses in rebar and coil conductors in response to unsteady or disturbed vehicle motion in the y- and z-directions.
It is assumed that a disturbance in the motion of the vehicle in the y or z-direction is superimposed on the steady-state motion in the x-direction. This disturbance gives rise to oscillatory motion of amplitude $\Delta\xi$ and frequency f and a corresponding oscillation in the amplitude of flux density δB at the site of a conductor in the guideway. Using Eqn. (3) for the large skin depth limit, and assuming only non-magnetic materials, the change in power dissipated per unit length of conductor is given by

$$\delta\langle P\rangle_T = 0.5\,\pi^3 r^4 \sigma f^2 \delta B^2 = 0.5\,\pi^3 r^4 \sigma f^2 \left(\frac{\partial B}{\partial \xi}\right)^2 \Delta\xi^2 \qquad (5)$$

where $\Delta\xi$ refers to a small displacement in the y or z –direction. If the response to the disturbance is harmonic, then the corresponding average value of the velocity over a half cycle is given by

$$v = 4 f \Delta\xi$$

and the estimated average value of the damping force per unit length of guideway conductor is given by the power dissipated divided by the average value of the velocity in the direction of the disturbance:

$$F_d\left(\frac{N}{m}\right) = \delta\langle P\rangle_T \Big/ v = K\left(\frac{\partial B}{\partial \xi}\right)^2, \qquad (6)$$

where

$$K = 0.125\,\pi^3 r^4 \sigma f \Delta\xi,$$

and the derivative of the B field with respect to y or z at the location of the guideway conductors was obtained numerically from the calculations of the B field described earlier.

The results of the damping force calculations at 4.77 Hz (30 rad/s) are given in Table 4 for oscillations in the z- or y-direction. The parameter values for cases 1, 2, & 3 are as shown in Table 2. The dominant damping force comes from the eddy currents induced in the null-flux coil conductors due to the number of conductors and their proximity to the SCM's. In this approximation, the damping force increases linearly with the oscillation amplitude and frequency. Notice that when the rebar and coil conductors are designed to reduce the drag forces as much as possible, the corresponding damping forces are also reduced proportionately.

Table 4 Approximate Damping Forces (N/ SCM) Associated With Eddy Current Losses in Guideway Components Caused By Vehicle Oscillations (ξ =0.01 m) in the z- or y-Direction at 30 (Rad./s).

	13%Mn Steel Rebar	Null-Flux Coils		Propulsion Coils
Direction of Oscillation	z	z	y	z
Case 1	0.182	26.9	48.5	4.0
Case 2	0.76	80.9	146	10.2
Case 3		3.5	6.3	0.48

4. Passive Damping Caused by Eddy Currents Induced in Vehicle-Borne Conductors by Motions Relative to Null-Flux Lift Coils

We now shift our attention from passive damping mechanisms involving the induction of eddy currents in guideway conductors to those involving the induction of eddy currents in vehicle-borne conductors. Conductors that are rigidly fixed to the vehicle and move relative to field sources located on the guideway and contribute to the passive damping of vehicle motions. Such conductors include closed-loop coils deliberately intended to serve as dampers, metallic plates that were intended to serve as eddy-current and thermal shields of superconducting magnets (SCM's) and power pickup coils. These coils and plates are exposed to the superposition of the constant primary fields from the vehicle SCM's, and time-varying fields due to the currents in the guideway coils, which are in motion relative to the vehicle. The time-varying part of the fields consist of a periodic variation associated with the longitudinal steady-state motion of the vehicle along the guideway and other field components associated with non-steady-state vehicle motions in the x, y, and z directions that are caused by perturbing forces.

Here we focus attention on the damping effects of cryostat walls that can be reasonably well simulated by shorted, single-turn coils. Fig. 2 shows the cross-sectional view of a SCM winding, an outer cryostat wall, a null-flux lift coil, and a propulsion coil. For computational simplicity, it will be assumed that all significant losses occur in the vertical outer wall. This ignores eddy current losses in the top, bottom, and end surfaces as well as the inner vessel walls.

A further simplification is to simulate each cryostat outer wall (or damping plate) with one or two "equivalent" damping coils as illustrated in Fig. 3. These "equivalent" damping coils are assumed to be shorted, single-turns in the same plane as the plates and made of the same material. The dimensions of the "equivalent" damping coils are difficult to determine precisely. As a first approximation, it will suffice to use the same thickness as the plates and coil shapes that closely resemble the shapes of the coils that serve as the field sources that cause the eddy currents. (A sensitivity analysis indicated that the results are not too sensitive to the dimensions of the "equivalent" coil). It is assumed that each SCM winding and its corresponding part of the cryostat wall spans three null-flux coils and three propulsion coils as illustrated in Fig. 1

Figure 2. Cross Sectional View of System Being Simulated

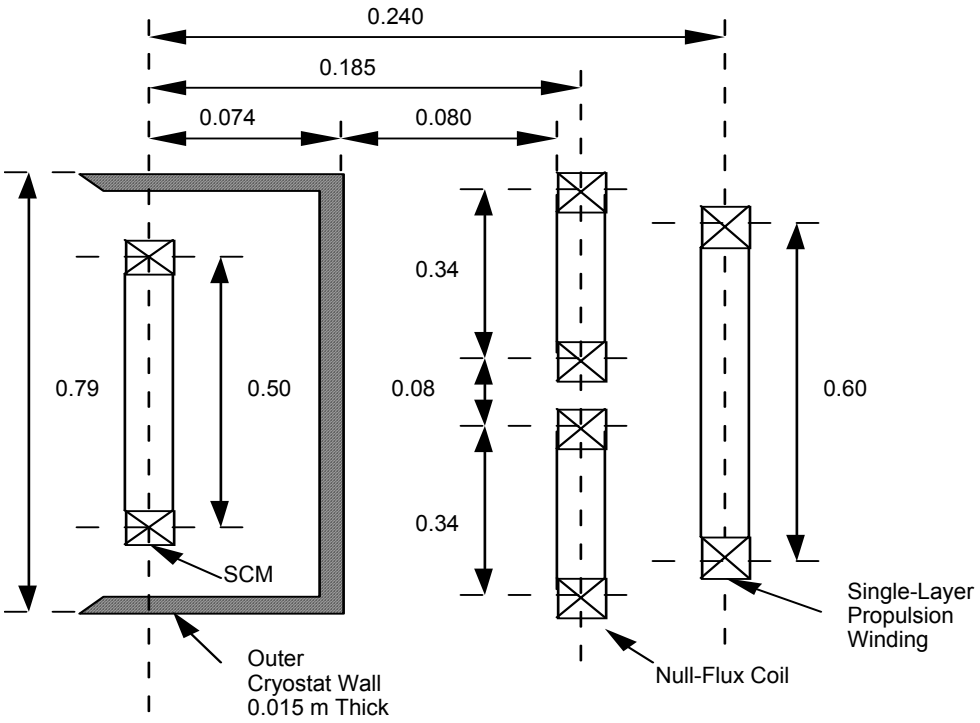

Figure 3. Shorted, Single-Turn Damping Coils Used to Simulate Damping Action of Damping Plate or Outer Cryostat Wall. For the Null-Flux Case An Upper and Lower Damping Coil is Used. For the Propulsion Coil Case a Single Damping Coil is Used.

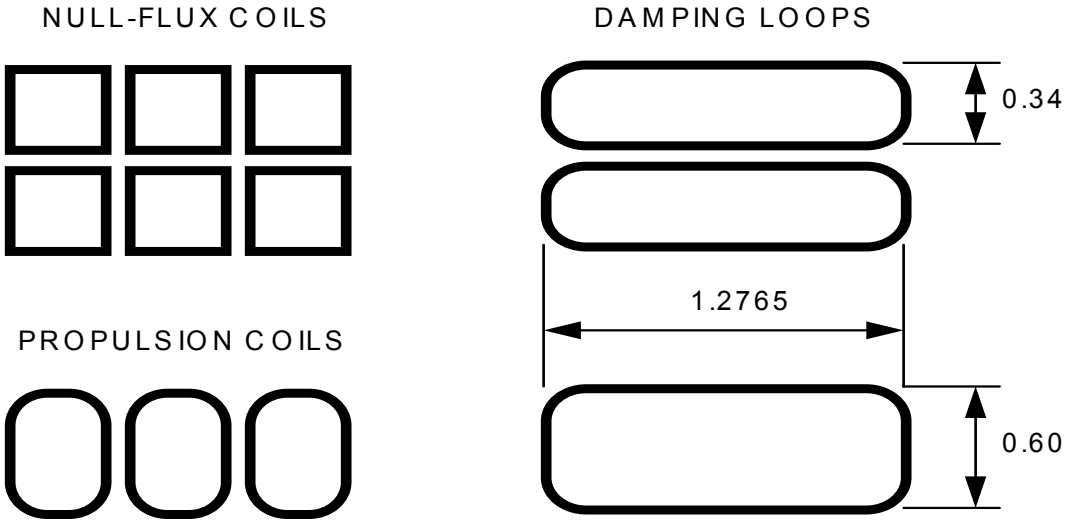

The method of analysis used here is based on the dynamic circuit model described in Refs. 2 & 3. Details will not be repeated here. The cases where the null-flux coils and the propulsion coils serve as the magnetic field sources are handled as though they were independent.

For the case where the null-flux coils are the source of the magnetic field, it is shown in Ref. 3 that the power dissipated in a damping loop oscillating in the vertical (z) direction is given by;

$$P_d = \frac{9}{16}\frac{V_z^2 I_s^2}{R_d}\frac{1}{1+\left(\frac{f_z}{f_c}\right)^2}\left\{\frac{1}{L_{geff}}\frac{\partial}{\partial z}\left[(M_{gl,s} - M_{gu,s})M_{d,g}\right]\right\}^2, \tag{8}$$

where V_z is the rms velocity in the z-direction, I_s is the current in the SCM, $M_{gl,s}$ is the mutual inductance between the lower null-flux loop and the SCM, $M_{gu,s}$ is the mutual inductance between the upper null-flux loop and the SCM, $M_{d,g}$ is the mutual inductance between the damping loop and the facing null-flux loop, L_{geff} is the self inductance of a null-flux loop, R_d and L_d are the resistance and effective self inductance of the damping loop, f_z is the frequency of oscillation in the z-direction, and the critical frequency f_c is defined by

$$f_c = \frac{R_d}{2\pi L_d}. \tag{9}$$

From Eqn. (8) we can identify the damping coefficient for motion in the z-direction as

$$C_z = P_d / V_z^2, \tag{10}$$

For the case where the propulsion coils are the source of the magnetic field, it is shown in Ref. 3 that the power dissipated in a damping loop oscillating in the vertical (z) direction is given by;

$$P_{dpz} = \frac{9}{16}\frac{I_p^2 V_z^2}{R_{dp}}\frac{1}{1+\left(\frac{f_z}{f_{cp}}\right)^2}\left[\frac{\partial}{\partial z}M_{d,p}\right]^2, \tag{11}$$

where I_p is the current in the propulsion coil, R_{dp} and L_{dp} are the resistance and self-inductance of the damping loop facing the propulsion coils, $M_{d,p}$ is the mutual inductance between the propulsion coil and the damping loop, and the critical frequency is defined as

$$f_{cp} = \frac{R_{dp}}{2\pi L_{dp}}. \tag{12}$$

For oscillations in the lateral (y) direction, replace the "z" with "y" in the above expressions.

In order to examine the damping coefficients associated with the null-flux coils as the field source, the term inside the curly brackets in Eqn. (8) can be expanded to

$$\frac{1}{L_{geff}}\left\{\frac{\partial}{\partial z}(M_{gl,s}-M_{gu,s})M_{d,g}+(M_{gl,s}-M_{gu,s})\frac{\partial}{\partial z}M_{d,g}\right\} \tag{13}$$

with a similar expression for the y-direction. At the null-flux position, $M_{gl,s} = M_{gu,s}$ so that the second term in Expression (13) vanishes. However, as is characteristic of null-flux systems, the derivative with respect to *z* of $(M_{gl,s} - M_{gu,s})$ is at a maximum at that position. Hence the first term is large and the damping in the z-direction is large. On the other hand, the derivative with respect to *y* of $(M_{gl,s} - M_{gu,s})$ is zero by symmetry, so that there is no damping of lateral motion at the null-flux position. As the vertical offset increases, both the first and second terms in Expression (13) contribute to the damping in both the y and z-directions. Similarly, when the propulsion coils are the field sources, symmetry indicates that at the null-flux position, the derivative of $M_{d,p}$ with respect to z is zero so that no vertical damping is provided at that position.

The parameter values used in the calculations described below are listed in Table 5.
The damping coefficients are shown in Figs 4 and 5 as a function of oscillation frequency, with the vertical offset from the null-flux position as a parameter.

Table 5 Parameter Values Used in Damping Calculations

	SCM Winding	Outer Cryostat Wall	Null-Flux Coil Loop	Simulated Damping Loop	Propulsion Coil Loop	Simulated Damping Loop
Length, X-Dir.	1.07	5.4	0.350	1.2765	0.3364	1.2765
Height, Z-Dir.	0.5	0.79	0.340	0.34	0.6	0.6
Thickness, Y-Dir.		0.015	0.038	0.015	0.0368	0.015
Width, XZ plane			0.079	0.079	0.0735	0.079
Winding Cross Sec.			0.003	0.0012	0.0027	0.0012
Series Turns			24	1	8	1
Parallel Windings			2			
Vertical spacing			0.080			
Horizontal Spacing			0.100			
Pole Pitch	1.35				1.35	
Conductivity (S/m)				3.53E+07	3.53E+07	3.53E+07
Resistance (m□)			8.34	0.0773	1.4	0.0897
Self Inductance (mH)			0.4054	0.00191	0.06398	0.002458
U-L Mutual Ind. (mH)			-0.0212			
Excitation (kA)	700				1.188	
Damping Coil Crit. Freq.*				6.4412		5.80806

*Sensitive to dimensions of coil used to simulate damping effects of damping plate
Coil dimensions are center-to-center of windings

For damped harmonic motion, the damping coefficient for a single damping loop is related to the exponential decay time through the equation

$$\tau_1 = 2M / C_\xi , \tag{14}$$

where M is the mass supported by a SCM coil. For a set of three null-flux coils there is one upper and one lower damping loop. Therefore, the decay time per set of three null-flux coils is

$$\tau_2 = M / C_\xi . \tag{15}$$

Now, what portion of the vehicle mass is allocated to each SCM coil?. In the case of the Japanese system at Yamanashi, there are eight SCM coils per bogie and one bogie per car. Hence, the appropriate value to use for the mass in Eqn. (15) is $M = M_C/8$, where M_C is the car mass, which is approximately 20 tons or 18144 Kg. Hence $\tau_2 = 2268 / C_\xi$. As indicated in Fig. 5, the maximum value of C_Z is about 500, at less than 1 Hz, which corresponds to a decay time of 4.5 s, which is quite long. As the vertical oscillation frequency increases, the decay time increases. Lateral decay times are longer still.

Again assuming damped harmonic motion, the damping coefficient can be related to the average damping force per damping loop and average velocity as follows:

$$\langle F_d \rangle = C V_{avg} = 4 C f \Delta \xi \tag{16}$$

Accounting for the number of damping loops per set of three null-flux coils (N = 2) and per set of three propulsion coils (N = 1), and the number of such coil sets per SCM (4), the average damping force per SCM is given by

$$\overline{F_d} = 16 N C_z f \Delta z . \tag{17}$$

The same expression applies to lateral damping force with the z's replaced with y's.
Using Eqn. (17), the average damping forces associated with these damping can be compared with the estimated damping forces associated with eddy currents induced in the guideway conductors (see Sec. 3.2). The results are summarized in Table 6 on a per SCM basis.

Note that in the case of the eddy currents induced in the guideway conductors, the dissipated power goes as the frequency squared and consequently the corresponding damping force goes as the frequency. In contrast, in the case of the currents induced in the vehicle-borne damping coils, the dependence on the oscillation frequency is more complicated. As Eqn. (16) shows, the damping force is proportional to V_{avg} ,which, in turn, goes as the frequency. However, the damping coefficient goes inversely as the frequency squared (see Figs. 4 and 5). Consequently, the damping force first increases then decreases with the frequency.

In the oscillation frequency range of interest, namely 1 to 10 Hz, Table 6 shows that the dominant vertical damping mechanism is the eddy currents induced in the simulated vehicle-borne damping plates by oscillations relative to the null-flux coils. In the null-flux position ($Z_0 = 0$), the largest damping in the lateral direction is due to the eddy currents induced in the large-radius null-flux coil conductors. For $Z_0 \neq 0$, that mechanism also produces the greatest lateral damping. However, if litz wire is used in the null-flux coils, then none of the mechanisms examined above produce very much lateral damping. Motion relative to the propulsion coils produces the least amount of damping of any of the damping mechanisms considered here.

Table 6 Comparison of Damping Forces per SCM (N/SCM) for Oscillation Amplitude of 0.01 m.

Oscillation Frequency (Hz)	**1**	**2**	**5**	**10**
Eddy Current Vertical Damping in Rebar				
Rebar Radius = 0.00794	0.004	0.008	0.19	0.38
Rebar Radius = 0.01588	0.16	0.32	0.80	1.6
Eddy Current Vertical Damping in Null-Flux Coil Conductors				
Conductor Radius = 0.00423	5.7	11.4	28.2	56.5
Conductor Radius = 0.00733	17.0	34.0	84.8	170
Conductor Radius = 0.00156	0.73	1.4	3.7	7.3
Eddy Current Lateral Damping in Null-Flux Coil Conductors				
Conductor Radius = 0.00423	10.2	20.4	50.9	102
Conductor Radius = 0.00733	30.6	61.2	153.0	306
Conductor Radius = 0.00156	1.3	2.6	6.6	13
Induced Current in Damping Plates Simulated by Shorted, Single -Turn Coils Due to				
Vertical Motion Relative to Null Flux Lift Coils				
$Z_0 = 0$ m	152	288	496	464
$Z_0 = 0.04$ m	104	200	336	320
Lateral Motion Relative to Null Flux Lift Coils				
$Z_0 = 0$ m	0	0	0	0
$Z_0 = 0.04$ m	32	59	104	96
Vertical Motion Relative to Propulsion Coils				
$Z_0 = 0$ m	0	0	0	0
$Z_0 = 0.04$ m	0.003	0.005	0.008	0.002
Lateral Motion Relative to Propulsion Coils				
$Z_0 = 0$ m	0.048	0.088	0.144	0.096
$Z_0 = 0.04$ m	0.044	0.080	0.128	0.064

Finally, an examination of the Eqns. (8) and (11) shows that the resistance of the damping coil enters these equations in the functional form

$$Q(R_d) = \frac{1}{R_d\left[1 + \left(f/f_c\right)^2\right]}. \tag{18}$$

Reducing R_d in this function increases Q at low frequencies and decreases it at high frequencies (f_c is proportional to R_d/L_d). Decreasing both R_d and L_d can produce larger values of Q over specified frequency ranges. This suggests that using a low self-inductance coil placed in a liquid nitrogen bath could produce larger damping than calculated here. This was in fact the strategy used at SRI[4] in the early seventies. In addition, a more exact treatment of the cryostat walls ia also expected to produce more damping than calculated here.

Figure 4a. Null-flux Coil – Damping Loop Lateral Damping Coefficient with Vertical Offset as a Parameter.

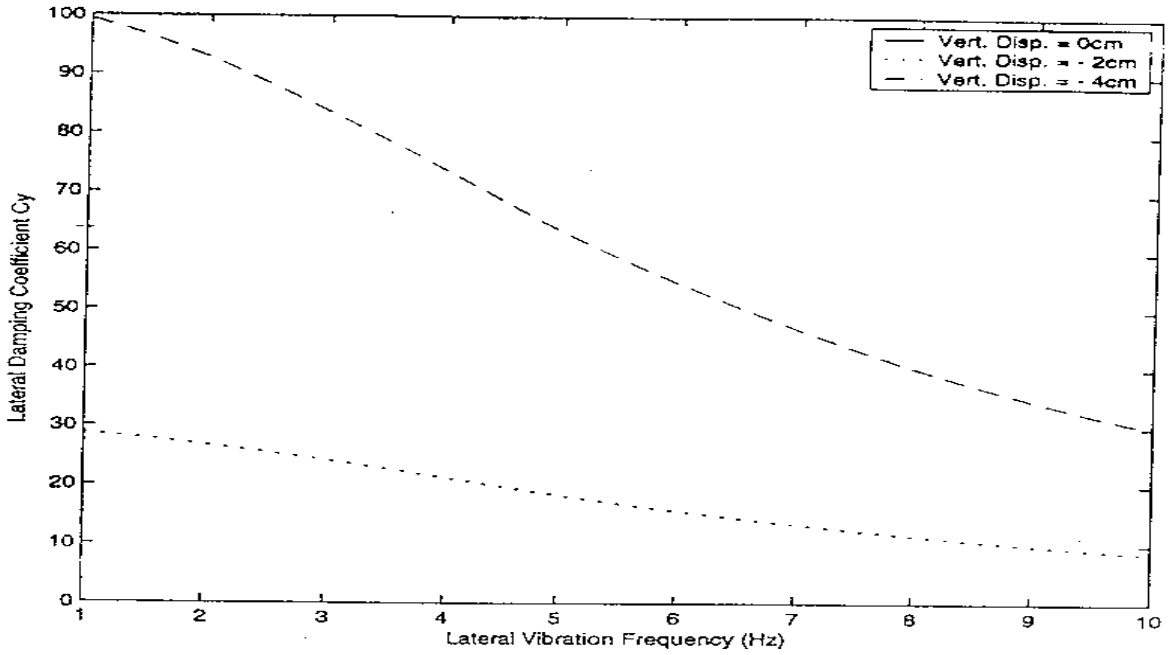

Figure 4b. Propulsion Coil – Damping Loop Lateral Damping Coefficient with Vertical Offset as a Parameter.

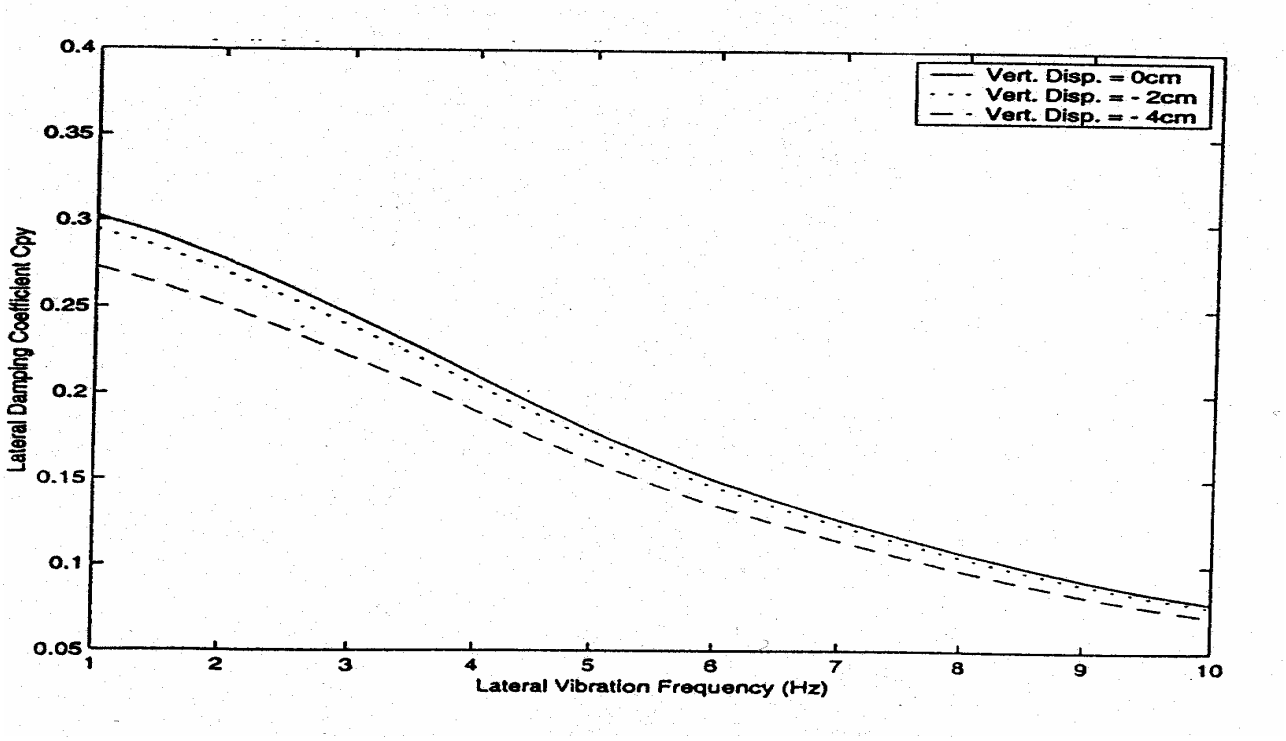

Figure 5a . Null-flux Coil – Damping Loop Vertical Damping Coefficient with Vertical Offset as a Parameter.

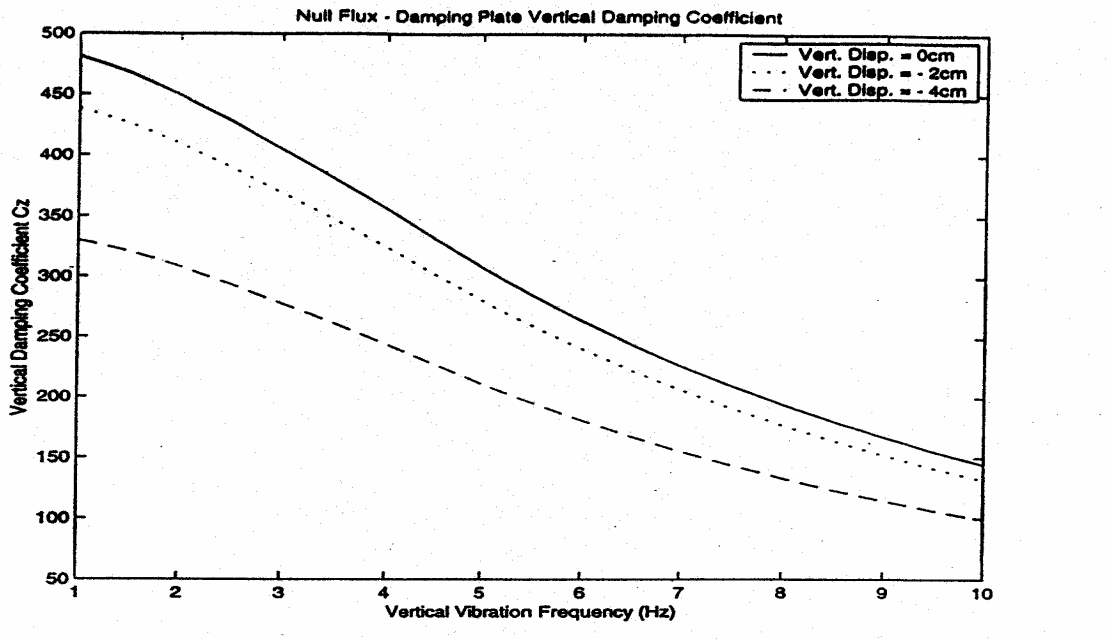

Figure 5b. Propulsion Coil – Damping Loop Vertical Damping Coefficient with Vertical Offset as a Parameter.

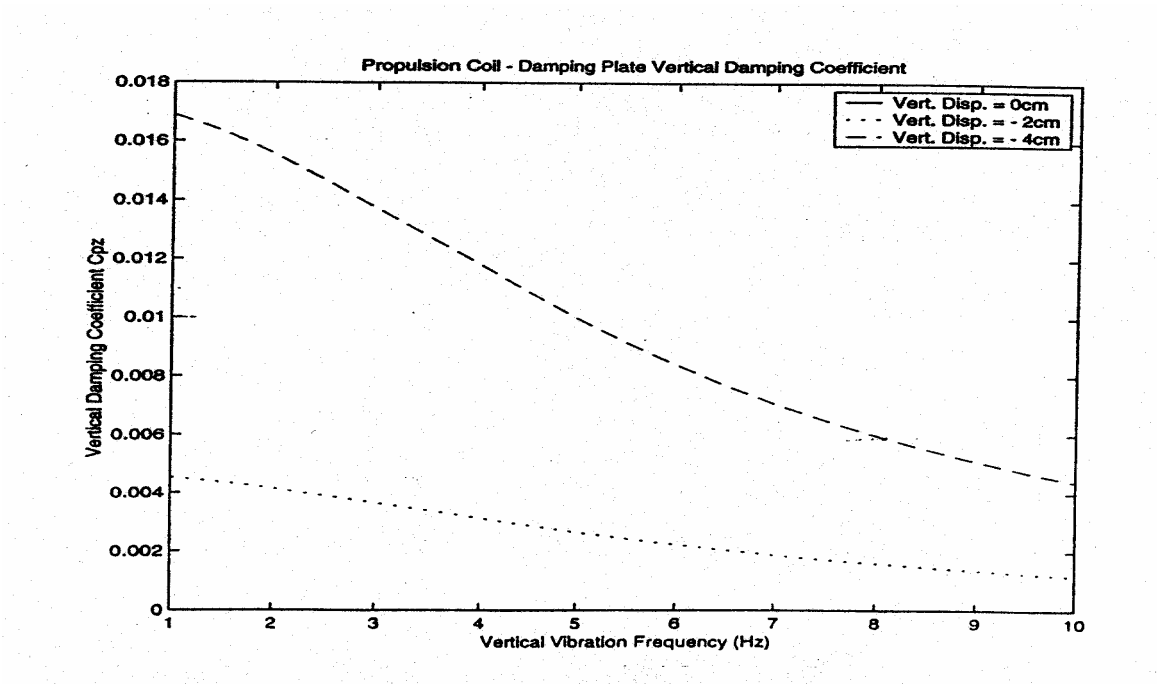

6. Conclusions

The focus of this paper was on estimating the relative importance of various sources of passive damping and drag forces in EDS systems. Two general mechanisms were considered. The induction of eddy currents in guideway-based electrical conductors, i.e. non-magnetic rebar, null-flux lift coil conductors, and propulsion coil conductors, and the induction of eddy currents in vehicle-borne damping coils, plates and cryostat walls.

It was shown that the drag force caused by eddy currents induced in guideway electrical conductors during steady-state vehicle motion in the x-direction increases with conductor radius and vehicle speed. In fact, these drag forces could become prohibitively large if conductor sizes were too large. It was also found that replacing thick coil conductors with stranded cables using individually insulated strands (i.e. litz wire) could substantially reduce the drag force. Unfortunately, the use of such cables also substantially reduced the damping forces. Tha damping forces caused by eddy currents induced in the guideway conductors by vehicle oscillations increased with both conductor size and frequency.

The other general damping mechanism involved the dissipation of eddy currents induced in vehicle-borne damping plates or cryostat walls by vertical and lateral motions relative to the null-flux lift and propulsion coils. Dynamic circuit theory was used to model the dynamic interactions between the SCM's, the guideway coils, and the damping plates, which were simulated by single, shorted-turn coils. The damping forces were found to peak in the frequency range of 1 to 10 Hz. In that frequency

range, the predominant damping was due to the eddy currents induced in the cryostat walls by motion relative to the null-flux coils. In fact, that was the overall dominant damping mechanism for vertical damping. However, that mechanism produced relatively less lateral damping and no lateral damping at all at the null-flux position. At the later position, the only significant source of lateral damping was eddy currents induced in large radius guideway conductors by oscillations of the SCM's. With small radius guideway conductors, there was very little lateral damping at the null-flux position.

The maximum vertical damping by the dominant mechanism was still relatively small, corresponding to a decay time of about 4.5s. Typically, one would like to see a decay time closer to 1 or 2s.

The absence of significant lateral damping at the null-flux position by any of the mechanisms examined (when small-radius conductors were used in the guideway) was an important finding for the null-flux lift coil-based maglev system. It suggests that for low-drag systems some form of active damping may be required.

Analysis indicated that one way to significantly enhance the passive damping mechanisms described above would be to significantly reduce the vehicle-borne damping coil resistance while at the same time reducing its self-inductance.

References

1. Zahn, M. Power Dissipation and Magnetic Forces on Maglev Rebar, Massachusetts Institute of Technology, Dept. of Electrical Engr. and Computer Science, prepared as a supplement to "Investigation of the Deleterious Effects of Electro-Magnetic Fields on Steel Rebar Used in Guideways for EDS Maglev Systems", Final Report, Volume 1, Summary, Oct 13, 1995, by R. D. Thornton, et al, to the Federal Railroad Administration.
2. He, Jianliang, and C. Coffey, Magnetic Damping Forces in Fig.-Eight-Shaped Null-Flux Coil Suspension Systems, presented at the INTERMAG 97 Conference, April 1, 1997.
3. Rote, D., Passive Damping in Repulsive-Force-Based Maglev Systems, Argonne National Laboratory Report No. ANL/ES/RP-106247, March, 2001.
4. Coffey, H. T., J. D. Colton, and K. D. Mahrer, Study of a Magnetically Levitated Vehicle, Final Report Task II, prepared for the Federal Railroad Administration, Report No. FRA-RT-73-24, Feb. 1973.